HHS Public Access

Author manuscript

Nat Biomed Eng. Author manuscript; available in PMC 2020 February 26.

Published in final edited form as:

Nat Biomed Eng. 2019 September ; 3(9): 695–705. doi:10.1038/s41551-019-0448-6.

Augmenting canonical Wnt signalling in therapeutically inert cells converts them into therapeutically potent exosome factories

Ahmed G.E. Ibrahim[1,2,*], **Chang Li**[1], **Russel Rogers**[1], **Mario Fournier**[1], **Liang Li**[2], **Sharon D. Vaturi**[2], **Travis Antes**[1], **Lizbeth Sanchez**[1], **Akbarshakh Akhmerov**[1], **Jennifer Johnson Moseley**[2], **Brooke Tobin**[2], **Luis Rodriguez-Borlado**[2], **Rachel R. Smith**[2], **Linda Marbán**[2,&], **Eduardo Marbán**[1,&,*]

[1]Smidt Heart Institute, Cedars-Sinai Medical Center, Los Angeles, CA, USA

[2]Capricor Therapeutics, Inc., Los Angeles, CA, USA

Abstract

Cardiosphere-derived cells (CDCs) are therapeutic candidates with disease-modifying bioactivity, but their variable potency has complicated their clinical translation. Transcriptomic analyses of CDCs from human donors have revealed that the therapeutic potency of these cells correlates with Wnt/β-catenin signalling and with β-catenin protein levels. Here, we show that skin fibroblasts engineered to overexpress β-catenin and the transcription factor Gata4 become immortal and therapeutically potent. Transplantation of the engineered fibroblasts into a mouse model of acute myocardial infarction led to improved cardiac function and mouse survival. And in the mdx mouse model of Duchenne muscular dystrophy, exosomes secreted by the engineered fibroblasts improved exercise capacity and reduced skeletal-muscle fibrosis. We also demonstrate that exosomes from high-potency CDCs exhibit enhanced levels of miR-92a (a known potentiator of the Wnt/β-catenin pathway), and that they activate cardioprotective bone-morphogenetic-protein

[*]Corresponding authors, ahmed.ibrahim@cshs.org.

Author contributions

AI: conceived the idea, designed experiments, performed experiments and data analysis, and wrote the manuscript.
CL, RR, MF, TA, and RS: performed experiments and provided technical and design input.
LL, SV, JM, BT, AA, and LS: performed experiments and data analysis.
LRB: assisted with project design.
LM: supervised the study.
EM: conceived the idea, wrote the manuscript and supervised the study.
[&]These authors supervised the project equally

Reporting summary. Further information on research design is available in the Nature Research Reporting Summary linked to this article.

Data availability

The authors declare that all data supporting the results in this study are available within the paper and its Supplementary Information.

Competing interests

Eduardo Marbán owns founder's stock in Capricor Therapeutics. Liang Li, Sharon Vaturi, Jennifer Moseley, Luis Rodriguez-Borlado, Rachel Smith, and Linda Marbán are employees of the company.

Supplementary information is available for this paper at https://doi.org/10.1038/s41551-01X-XXXX-X.

Publisher's note: Springer Nature remains neutral with regard to jurisdictional claims in published maps and institutional affiliations.

signalling in cardiomyocytes. Our findings show that the modulation of canonical Wnt signalling can turn therapeutically inert mammalian cells into immortal exosome factories for cell-free therapies.

EDITORIAL SUMMARY

Overexpression of β-catenin and the transcription factor Gata4 in skin fibroblasts converts them into therapeutically active cells that secrete reparative exosomes as shown in mice models of myocardial infarction and Duchenne muscular dystrophy.

Cardiosphere-derived cells (CDCs) trigger repair and functional improvement after injury to heart[1, 2] and skeletal[3] muscle. Several early-stage clinical trials of CDCs have shown benefits on surrogate markers of disease progression in acquired[4] or congenital[5] forms of heart failure. Mechanistic preclinical studies reveal that CDCs exert their benefits indirectly, by secreting exosomes and other extracellular vesicles (EVs) that stimulate anti-inflammatory, antifibrotic, angiogenic, and cardiomyogenic pathways[6]. Nevertheless, therapeutic potency remains inconsistent: CDCs and other primary cell types[7, 8] exhibit variable potency across donors[9], and process improvement efforts can also inadvertently undermine potency[10]. Mechanistically-based strategies to increase potency are lacking, but highly desirable[11].

For cardiac applications of cell therapy, the gold standard potency assay measures functional and/or structural recovery *in vivo* after myocardial infarction (MI) in rodents[9]. The continuing reliance on this costly, low-throughput model reflects a poor mechanistic understanding of the molecular determinants of potency. Here we systematically compared high- and low-potency human CDCs at transcriptomic, translational, and functional levels. The emergent insights not only include previously-unrecognized markers of CDC potency, but also strategies to enhance the therapeutic efficacy of CDCs, of other cell types, and of secreted exosomes.

Results

Implication of Wnt/β-catenin signaling in CDC potency

Variable therapeutic efficacy is evident among various human CDC lines subjected to *in vivo* testing post-MI. Fig. 1a shows the changes in global heart function, quantified echocardiographically as ejection fraction (EF), from mice injected with each of four high-potency (HP) human CDC lines, four low-potency (LP) lines (selected for sequencing), or vehicle only (saline). Transcriptomic comparison of HP and LP CDCs revealed differentially-expressed Wnt signaling mediators, with activation of β-catenin signaling in HP CDCs (Fig. 1b). In contrast, non-canonical Wnt pathway members ror2, nfatc2, axin2, rac2, and apcdd1 were enriched in LP CDCs (Fig. 1c), while little difference was evident in several molecules that are shared by canonical and non-canonical Wnt signaling pathways (Frizzled receptors (Fig. 1d), Dishevelled, (Fig. 1e) and Wnt ligands (Fig. 1f)).

The RNA sequencing results motivated us to examine the relationship between Wnt/β-catenin signaling and CDC potency. Pooled data for donor-specific total β-catenin protein

levels in CDCs revealed a strong correlation with therapeutic efficacy of the same cells *in vivo* (Fig. 2a). All CDCs were from putatively healthy donor hearts which had passed standard minimal criteria for human transplantation (including screening for infectious diseases) but had not been used for a technical reason (e.g., heart size, blood type) and thus were donated for research. No discernible correlation was found between clinical characteristics of donors (i.e. age, sex, ethnicity, or cause of death) and the observed potency of CDCs. HP CDCs exhibited ~2-fold higher β-catenin levels, on average, compared with LP CDCs. Wnt receptor expression, including low-density lipoprotein receptor 5/6 (LRP5/6), promotes stabilization of cytoplasmic β-catenin and prevents its ubiquitination[12]. Wnt receptors LRP5/6 were elevated in HP CDCs (Fig 2b). Furthermore, the sphere-forming transition, central to the preparation of CDCs, involves a dramatic decrease then sharp rise of β-catenin levels in the CDCs thereafter (though variability among donors was observed) (Supplementary Fig. 1a).

Boosting β-catenin enhances potency

To test whether boosting β-catenin levels would improve therapeutic efficacy in LP CDCs, we used 6-bromoindirubin-3'-oxime (BIO), a reversible inhibitor of glycogen synthase kinase-3 beta (GSK3β) which is maximally effective in CDCs at 5 μM (Supplementary Fig. 1b). By releasing GSK3β's suppressive effect, BIO can increase β-catenin levels, which was indeed what we observed in a LP line exposed to BIO (LP-BIO, Fig. 2c). BIO decreased the expression of CD90, an antigen which correlates inversely with potency[9, 13], without affecting the positive CDC identity marker CD105 or the negative identity marker DDR2 (Supplementary Fig. 1c). Tideglusib, an irreversible inhibitor of GSK3β, had directionally similar but longer-lasting effects (Supplementary Fig. 1d, e). LP-BIO CDCs showed enhanced functional and structural benefits compared to unexposed LP CDCs (LP-Vehicle) (Fig. 2d–g). Enhancement of β-catenin did not affect the persistence of transplanted CDCs in host cardiac tissue (Supplementary fig. 2a).

Although donor-to-donor variability in potency is most common, we occasionally find that, for unclear reasons, different lots from the same master cell bank can differ in potency. Fig. 2h shows that β-catenin levels increase when LP lots (LPL) are exposed to BIO (LPL-BIO),and do so to levels comparable to HP lots (HPL) from the same donor. Such "corrected" lots also regain therapeutic efficacy *in vivo* (Fig. 2i). Finally, we have found that CDCs immortalized using simian virus 40 large and small T antigen (SV40 T+t) are not potent and exhibit low levels of β-catenin, but regain potency following β-catenin augmentation by exposure to BIO (Fig. 2j, k). Thus, in three different scenarios—donor-to-donor variability, lot-to-lot variability, and immortalization—boosting CDC β-catenin levels increases cell potency.

Mest inhibits β-catenin through inhibition of LRP5/6 receptor expression

To understand how β-catenin drives potency, we compared the transcriptomes of LP CDCs to those of the same cell batches after exposure to BIO. As stated above, we have identified three scenarios associated with low potency: donor-related, in which all lots from a given donor lack potency; lot-dependent, in which some lots are potent and others are not; and immortalized CDCs (imCDCs). Using RNA sequencing, LP cells from each scenario were

compared after exposure to BIO versus vehicle alone. Fold changes were then pooled to identify genes up- or down-regulated by BIO (Fig. 3a). In addition to the many promoters of canonical Wnt signaling which were up-regulated, one basal negative regulator of Wnt signaling, mesoderm-specific transcript (mest), was strikingly downregulated (~30-fold; Fig. 3b, c; Supplementary Fig. 2b, c). Differential expression of microRNAs (miRs) between the two groups further identified a cognate miR coregulated with mest (miR-335; Fig. 3c, Supplementary Fig. 2d, e). Overexpressing β-catenin in fibroblasts increased mest expression, suggesting that β-catenin-mediated mest inhibition is cell autonomous (Supplementary Fig. 2f). Mest modulates Wnt/β-catenin signaling indirectly through glucosyltransferases that prevent LRP5/6 receptor maturation[14]. Mutations in members of the exostosin (EXT) family of glucosyltransferases affect Wnt receptor pattern expression during development[15]. Here, LRP5/6 transcripts were unchanged with downregulation of the exostosin glycosyltransferase EXTL1, confirming that mest and EXTL1 inhibit LRP5/6 post-transcriptionally[14] (Fig. 3f–h). In further support of a mechanistic link, CDC exposure to BIO decreased EXTL1 protein levels (Fig. 3i; Supplementary Figure 10a, b) and upregulated its glycosylation target LRP5/6 (although that difference was not statistically significant; Fig. 3j).

Given the importance of exosomes, and possibly other EVs, as mediators of the therapeutic benefits of CDCs, we investigated EV properties and effects. Despite similar levels of previously-identified positive and negative therapeutic miRs (146a[16, 17] and 199b[17] respectively), and similar size distribution profiles, of EVs produced by plus/minus BIO cell pairs (Supplementary Fig. 3a, b), EV levels of miR-335 decreased significantly, demonstrating modulation of noncoding RNA payload by β-catenin activation (Fig. 3d). Fibroblasts exposed to HP CDC EVs exhibited downregulated mest levels compared to those exposed to fibroblast EVs or LP CDC EVs (Fig. 3e). Therefore, β-catenin activation leads to mest/miR-335 repression in potent CDCs and decreases miR-335 in their secreted EVs.

Genetic suppression of mest in immortalized CDCs

Initial attempts at immortalizing CDCs relied on simian virus 40 large and small T antigen transduction. As expected, using SV40 large and small (T+t) antigen led to a change in morphology towards a spindle-like morphology[18, 19], and robust growth[17] past the expected ~8 passages post sphere formation (Supplementary Fig. 4a)[9]. Surface marker expression remained largely similar except for a sharp rise in CD90, a previously-identified negative marker of potency in CDCs (Supplementary Fig. 4b)[13]. EV size was similar (Supplementary Fig. 4c) but EV output was increased; this is a common consequence of primary cell immortalization[20] (Supplementary Fig. 4d). Finally, levels of known therapeutic CDC EV cargo components, notably miR-146a and miR-210 (see refs[17] and[16]), fell in comparison to primary CDC EVs (Supplementary Fig. 4e). Therefore, while this strategy succeeded in immortalizing CDCs, it led to a loss of potency (Fig. 2j, k) and attenuation of β-catenin levels (Fig. 4a). Although BIO restored potency in immortalized CDCs (Fig. 2j, k), cell growth and viability were undermined (Supplementary Fig. 4f). In another attempt to restore potency to immortalized CDCs, knockdown of GSK3β led to transcriptional repression (Supplementary Fig. 5a) and paradoxical downregulation of β-catenin (Supplementary Fig. 5b). As observed with pharmacological inhibition of GSK3β, transcriptional repression of

GSK3β also led to mest downregulation (Supplementary Fig. 5b). Repression of β-catenin expression is not surprising given known homeostatic mechanisms. Gsk3a and gsk3b have functional redundancies, such that blocking gsk3b leads to inhibition of gsk3b-mediated effects; genetic deletion of gsk3b abrogated those effects due to compensatory activation of gsk3α[21]. Genetic suppression of mest using a short hairpin (sh) RNA yielded better results: EXTL1 protein levels decreased, and surface expression of LRP5/6 increased (Fig. 4b, c; Supplementary Figure 11a–c), such that imCDC$^{sh\text{-}mest}$ cells maintained high β-catenin levels (comparable to those of potent CDCs) for at least 20 passages (Fig. 4d). While potent therapeutically, imCDC$^{sh\text{-}mest}$ differed from primary CDCs in morphology and identity markers (Supplementary Fig. 5c–d). EVs were produced by imCDC$^{sh\text{-}mest}$ (Supplementary Fig. 6a, b), and those EVs contained higher miR-146a and lower miR-199b levels than primary CDC EVs (Fig. 4e). Finally, imCDC$^{sh\text{-}mest}$ exhibited high potency both structurally (by reductions in histological scar size; Fig. 4f–h) and functionally *in vivo* (Fig. 4i).

Engineering therapeutic potency into a non-potent, non-cardiac cell type

Having shown that β-catenin underlies CDC potency, we questioned whether β-catenin overexpression could induce potency in a therapeutically-ineffective cell type, normal human dermal fibroblasts (NHDFs). We studied β-catenin enhancement with and without co-expression of gata4 (Fig. 5a), a transcription factor which signals downstream of Wnt/β-catenin during cardiac development[22] and enhances the cardioprotective potential of mesenchymal stem cells[23]. Comparison of NHDFs, NHDFs transduced with β-catenin only (NHDF$^{\beta cat}$), and NHDFs transduced with both β-catenin and gata4 (NHDF$^{\beta cat/gata4}$) revealed clear morphological differences, with NHDF$^{\beta cat}$ and NHDF$^{\beta cat/gata4}$ cells having endothelial- and epithelial-like morphologies, respectively (Fig. 5b). In NHDF$^{\beta cat/gata4}$, we further observed a lack of senescence akin to immortalization. Indeed, telomerase expression was markedly increased in these cells, pointing to a possible synergy between β-catenin and gata4 in cell growth (Supplementary Fig. 7a). Among transcription factors, gata4 is at least somewhat specific in its effects: substituting gata4 with the endothelial cell-fate transcription factor, etv2[24], did not recapitulate the immortalized phenotype (Supplementary Fig. 7b). Relative to unmodified NHDFs, antigenic profiling revealed decreases in CD90 and CD105 in NHDF$^{\beta cat}$, and almost complete loss of these markers in NHDF$^{\beta cat/gata4}$ (Fig. 5c). β-catenin levels were increased in both NHDF$^{\beta cat}$ and NHDF$^{\beta cat/gata4}$ relative to unmodified NHDFs (Fig. 5d) likely due to silencing of β-catenin during cell-fate specification[25, 26]. EVs derived from NHDF$^{\beta cat}$ and NHDF$^{\beta cat/gata4}$ expressed increased levels of miR-146a; however, only NHDF$^{\beta cat/gata4}$ showed reduced miR-199b (Supplementary Fig. 7c; Fig. 5e). To assess therapeutic efficacy, we quantified mortality and heart function post-MI. Fig. 5f shows that NHDFs are actually deleterious, not just inert, after transplantation; they hinder survival, insofar as >50% of NHDF-injected animals died by the third week post-MI. Lower mortality was observed in mice injected with NHDF$^{\beta cat}$ or NHDF$^{\beta cat/gata4}$; indeed, all animals survived in the latter group, and also in a group injected with EVs from NHDF$^{\beta cat/gata4}$ (Fig. 5f). Similar patterns characterized the cells' capacity to improve EF post-MI (Fig. 5g–i). Given these findings, we dubbed the engineered cells and their EVs/exosomes Activated-Specialized Tissue Effector Cells (ASTECs) or ASTEX, respectively.

Engineered fibroblasts (or their EVs), ASTECs (or ASTEX), may have therapeutic utility beyond the heart. To probe the bioactivity more generally, we tested ASTEX in a murine model of Duchenne muscular dystrophy by injecting *mdx* mice with 3×10^9 particles (or vehicle only) intravenously (Fig. 6a). Three weeks later, ASTEX-injected mice (but not controls) ran significantly further than at baseline (Fig. 6b). Histological examination of the *mdx* mouse tibialis anterior, a prototypical fast-twitch skeletal muscle, revealed greatly reduced muscle fibrosis in ASTEX relative to control (Fig. 6c, d). Meanwhile, ASTEX shifted myofiber size distribution to larger diameters (Fig. 6e), mimicking the effects of CDC-derived exosomes in this model[3]. Together, these data indicate that ASTEX are bioactive not only in ischemic heart failure (Fig. 5g) but also on dystrophic skeletal muscle.

MiR-92a-bmp2 signaling axis underlies β-catenin activation

One theoretical mechanism would posit that β-catenin-activated CDCs simply increased β-catenin levels in the injured myocardium when injected. To test whether myocardial activation of β-catenin is cardioprotective, we administered drugs to alter global canonical Wnt signaling systemically in mice with MI, independent of CDCs. Neither BIO nor the canonical Wnt inhibitor JW67 significantly altered myocardial function relative to controls (Supplementary Fig. 8a), divorcing global myocardial alterations in Wnt signaling from the effects of CDCs. Instead, transcriptomic analysis in a reductionist *in vitro* model (using neonatal rat ventricular myocytes; Supplementary Fig. 8b, c) revealed major changes in the bone morphogenic peptide (BMP) family of genes after exposure to HP CDC EVs. BMP genes are central regulators of cardiac fibrosis; moreover, bmp2 is a target of β-catenin[27–29] and promotes myocyte contractility[30, 31]. Differentially-expressed BMP family members include anti-fibrotic bmp- 2, its receptor (2r), −6, and 8a, all of which were upregulated, while profibrotic members, including bmp −3, −4, GDF6, and 10, were suppressed (Fig. 7a, b). Furthermore, fibroblasts exposed to HP EVs upregulate bmp2 compared to fibroblasts exposed to their own EVs or LP-EVs (Fig. 7c). A microRNA coregulated with bmp2, miR-92a, promotes bmp2 signaling[32, 33]. Indeed miR-92a is enriched in HP EVs compared to LP EVs (Fig. 7d). Consistently, miR-92a is also enriched in the EVs of imCDC^{shmest} as well as ASTEX (Fig. 7e, f).

Discussion

Wnt signalling comprises three highly evolutionarily-conserved pathways; one canonical, which regulates transcription, and two non-canonical, which regulate cell structure and calcium handling[34]. Here we have shown that canonical Wnt signalling is enriched in potent CDCs, whereas non-canonical Wnt signalling is enriched in non-potent CDCs. β-catenin, which is the nodal point of canonical Wnt signalling, is known to be involved in_ endometrial regeneration[35]. During the healing phase, β-catenin subsides and CD90 levels increase in stromal tissue[35]. β-catenin signalling figures prominently in a number of related pathophysiological pathways including pro-reparative macrophage polarity[36–38], attenuation of fibrosis[39–41], cardiomyogenesis[22, 42–44], and angiogenesis[45–47]. Furthermore, cardiac preconditioning is associated with accumulation of β-catenin and its downstream cascade[48]. β-catenin overexpression reduces MI size through effects on cardiomyocytes and cardiac fibroblasts[49]. We find that β-catenin is not only a potency marker but also mechanistically

critical to therapeutic efficacy. Mest is a critical turning point to non-canonical Wnt signalling through regulation of LRP5/6 expression and activation of EXTL1 (Fig. 7g). β-catenin transcriptionally inhibits mest and extl1, likely through the activity of downstream gene targets, though the exact mechanism remains unknown.

Our findings are consistent with the working hypothesis that activation of β-catenin in CDCs leads to enrichment of its coregulated miR, miR-92a, which in turn leads to improved contractility and attenuation of fibrosis in target tissue (Fig 7h). The present findings motivate further mechanistic dissection, including elucidation of precisely how β-catenin represses the mest-extl1 axis. In any case, the role of canonical Wnt signalling appears to be generalizable beyond CDCs, insofar as we have successfully converted deleterious fibroblasts into therapeutically-beneficial engineered novel cell entities (ASTECs) by manipulating β-catenin. The mechanistic findings on CDC potency informed our efforts to create ASTECs: immortal, defined cells engineered to have disease-modifying bioactivity. From a product development viewpoint, ASTECs are notable not only because such cells may, themselves, be viable therapeutic candidates, but also because they constitute a well-defined, immortal source for manufacturing high-potency exosomes and other EVs. As reviewed[11, 50], EVs offer the potential to overcome key limitations of cell therapy. Cells are sensitive and labile living entities, vulnerable to even to minor changes in manufacturing conditions. This renders their manufacturing and scalability costly and logistically burdensome[51]. EVs are non-living, stable, and hardy. As small bilayer vesicles, they can tolerate lyophilization, repeated freeze-thaw cycles, and other harsh handling methods whilst remaining bioactive[52]. Another advantage of their size is the safety of higher dose thresholds and broader penetration into tissue (e.g., crossing the blood-brain barrier) without the concern of microvascular occlusion or viability loss[53]. Furthermore, EVs, unlike their parent cells, exhibit immune versatility, exerting their therapeutic effects even in xenogeneic contexts. Human exosomes have been shown to induce therapeutic benefits in mice[3], rats[54, 55], and pigs[56]. ASTEX have all these theoretical advantages. Unlike previous efforts to derive EVs from immortalized cells[20], ASTEX further have the distinction of having been created by mechanistically-informed genetic engineering of the parent cells to enhance their therapeutic efficacy.

Methods

Cells and reagents.

Endomyocardial biopsies from the right ventricular aspect of the interventricular septum were obtained from the healthy hearts of deceased tissue donors. CDCs were derived as described previously[2]. Briefly, heart biopsies were minced into small 1 mm^2 fragments and digested briefly with collagenase. Explants were then cultured on 20 μg/ml fibronectin (VWR)-coated flasks. Stromal-like, flat cells, and phase-bright round cells grew spontaneously from the tissue fragments and reached confluence by two to three weeks. These cells were then harvested using 0.25% trypsin (GIBCO) and cultured in suspension on 20 μg/ml poly-D-lysine (BD Biosciences) to form self-aggregating cardiospheres. CDCs were obtained by seeding cardiospheres onto fibronectin-coated dishes and passaged. All cultures were maintained at 5% O_2/CO_2 at 37°C, using IMDM basic media (GIBCO)

supplemented with 10% FBS (Hyclone), 1% Gentamicin, and 0.1 ml 2-mercaptoethanol. Human heart biopsy specimens, from which CDCs were grown, were obtained under a protocol approved by the institutional review board for human subjects research.

Extracellular Vesicle preparation and isolation.

Extracellular Vesicles were harvested from primary CDCs at passage 5 or older passages from transduced cells using a hypoxic cycling method used previously by our group[3]. Briefly, cells were grown to confluence at 20% O_2/5% CO_2 at 37°C, and then cells were serum-free at 2% O_2/5% CO_2 at 37°C overnight after one wash. Conditioned media was collected and filtered through 0.45 μm filter to remove apoptotic bodies and cellular debris and frozen for later use at −80°C. EVs were purified using centrifugal ultrafiltration with a 1000 KDa molecular weight cutoff filter (Sartorius). EV preparations were analyzed through Malvern Nanosight NS300 Instrument (Malvern Instruments) with the following acquisition parameters: camera levels of 15, detection level less than or equal to 5, number of videos taken 4, and video length of 30 s.

Lentiviral transduction.

CDCs or NHDFs were plated in T25 flasks and transduced with lentiviral particles (MOI: 20) in complete media. After 24 hrs transduction, virus was removed, and fresh complete media was added for cell recovery for a further 24 hrs. Cells were then subjected to selection media for approximately one week. Following selection complete media was replaced.

RNA isolation and qRT-PCR.

Cell RNA was isolated using miRNeasy Mini Kit (Qiagen). Exosome RNA was isolated using the Urine Exosome RNA Isolation Kit (Norgen Biotek Corp.). Reverse transcription was performed using High Capacity RNA to cDNA (Thermo Fisher Scientific) or TaqMan® microRNA Reverse Transcription Kit (Applied Biosystems) for RNA and micro RNA respectively. Real-time PCR was performed using TaqMan Fast Advanced Master Mix and the appropriate TaqMan® Gene Expression Assay (Thermo Fisher Scientific). Samples were processed and analyzed using a QuantStudio™ 12K Flex Real-Time PCR system and each reaction was performed in triplicate samples (with housekeeping genes hprt1 for mRNA and miR23a for microRNA). The gene expression assays/microRNAs used in this study are summarized in Supplementary Table 1.

RNA sequencing.

Cell and exosome RNA samples were sequenced at the Cedars Sinai Genomics Core. total RNA and Small RNA were analyzed using an Illumina NextSeq 500 platform for cell and exosome samples respectively.

Western blot.

Membrane transfer was performed using the Turbo® Transfer System (BIO-RAD) after gel electrophoresis. The following antibody staining was then applied and detected by SuperSignal™ West Pico PLUS Chemiluminescent Substrate (Thermo Fisher Scientific). Antibodies used in this study are summarized in Supplementary Table 2.

Cell lysate and protein assay.

Cell lysates were collected for ELISA and western blot. For ELISA, 4×10^5 cells were collected and pelleted at 1,000 rpm for 5 min at 4°C. Cell pellets were lysed in 1x lysis buffer (Affymetrix eBioscience InstantOne ELISA kit) and incubated for 10 min at room temperature with regular agitation. For western blot, cells of were pelleted and resuspended in 1x RIPA buffer (Alfa Aesar) with protease inhibitor on ice for 30 min. Protein lysates were isolated by centrifugation at 14,000 rpm for 15 min at 4°C. Protein concentration was measured using a DC™ Protein Assay kit (Bio-Rad).

Drug exposure of cells.

Cells were exposed to 5 μM of 6-bromoindirubin-3'-oxime (BIO, Sigma-Aldrich) or 4-Benzyl-2-(naphthalen-1-yl)- [1,2,4] thiadiazolidine-3,5-dione (Tideglusib, Sigma-Aldrich) for 48 or 72 hours in complete media.

ELISA.

Total β-catenin ELISA was performed according the protocol described with a final sample concentration of 0.01 mg/ml and positive control of 0.1 mg/ml (Affymetrix eBioscience InstantOne™ ELISA).

Flow cytometry.

Cells were harvested and counted (2×10^5 cells per condition). Cells were washed with 1% bovine serum albumin (BSA) in 1x phosphate-buffered saline (PBS) and stained with the appropriate antibody (BD Pharmingen) for 1 hr at 4°C. Cells were then washed again and resuspended in 1% BSA in 1x PBS. BD Cytofix/Cytoperm™ kit was used for cell permeabilization before staining. Flow analysis was done using a BD FACS Canto™ II instrument or Sony SA3800. Gating strategy is outlined in Supplementary Figure 9.

Animal Study.

All animal studies were conducted under approved protocols from the Institutional Animal Care and Use Committee protocols.

Mouse Acute MI model.

Acute myocardial infarction was induced in three-month-old male severe combined immunodeficient (SCID)/beige mice as described (n=5–7 animals per group)[8]. Within 10 min of coronary ligation, 1×10^5 cells, EVs, drugs (or vehicle) were injected intramyocardially.

Echocardiography.

Echocardiography study was performed in the SCID/beige at 24 hr (baseline) and three weeks after surgery using Vevo 3100 or 770 Imaging System (Visual Sonics) as described[8]. The average of the left ventricular ejection fraction was analyzed from multiple left ventricular end-diastolic and left ventricular end-systolic measurements.

CDC Engraftment.

To assess human CDC persistence, infarcted animals received LP CDCs pre-exposed to 5 μM of BIO or an equivalent volume of DMSO 72 hours prior to injection. A standard curve was made using copy numbers of the human X-chromosome specific gene mage a1. DNA from known numbers of this CDC donor in DNA from 1 mg of mouse cardiac tissue was used to make the standard curve. Three weeks post-injection animals were sacrificed, and genomic DNA was extracted from ventricular tissue. QPCR of mage a1 copy number in genomic DNA was done using a Taqman Copy Number Assay (Thermo Fisher Scientific).

Histology.

Animals were sacrificed 3 weeks after MI induction. Hearts were harvested and a transverse cut was made slightly above the MI suture. The apical portion was then embedded in optimum cutting temperature solution in a base mold/embedding ring block (Tissue Tek). Blocks were immediately frozen by submersion in cold 2-methylbutane. Hearts were sectioned at a thickness of 5 μm.

Masson's Trichrome Staining.

Two slides containing a total of four sections per heart were stained using Masson's trichrome stain. In brief, sections were treated overnight in Bouin's solution. Slides were then rinsed for 10 min under running water and stained with Weigert's hematoxylin for 5 min. Slides were then rinsed and stained with scarlet-acid fuchsin for 5 min and rinsed again. Slides were then stained with phosphotungstic/phosphomolybdic, aniline blue, and 2% acetic acid for 5 min each. Slides were then rinsed, dried, and mounted using DPX mounting media.

Duchenne muscular dystrophy mouse model

Treadmill Exercise Testing: Ten-month-old female *mdx* mice were placed inside an Exer-3/6 rodent treadmill (Columbus Instruments) equipped with a shock grid elevated 5 degrees. During the acclimatization period, mice were undisturbed for 30 min prior to engagement of the belt. After the belt engaged, mice were encouraged to familiarize themselves with walking on the treadmill at a pace of 10 m/min for an additional 20 min. After the acclimatization period, the exercise protocol engaged (shock grid activated at 0.15 mA with a frequency of 1 shock/sec). This protocol is intended to induce volitional exhaustion by accelerating the belt speed by 1 m/min every minute. Mice that rest on the shock grid for >10 s with nudging were considered to have reached their maximal exercise capacity (their accumulated distance traveled is recorded) and the exercise test was terminated. Animals were tested at baseline then later in the day received 100 μl intravenous (femoral vein) infusions of exosomes or saline vehicle. Animals were tested one more time three weeks post infusion.

Histology: The mouse tibialis anterior (TA) muscles were dissected freely from anesthetized mice and embedded in OCT compound and frozen in 2-methylbutane pre-cooled in liquid nitrogen, then stored at −80°C until sectioning. Serial sections were cut at the mid-belly in the transverse plane. All sections were cut at 8 μm using a cryostat (Leica) and adhered to

Superfrost Plus™ microscope slides (Fisherbrand). Cryosections were fixed with 10% neutral buffered formalin for 10 min prior to Masson's trichrome staining (Sigma-Aldrich). Histological slides were imaged using an Aperio AT Turbo slide scanner (Leica) at 40x magnification. Quantification of fibrosis was determined by the area of blue staining relative to red staining of the entire tissue section using Tissue IA (Leica Biosystems). Feret diameter was measured on 1,000 myofibers per section using QuPath software integrated with ImageJ.

Statistical Analysis: Statistical Comparisons were made using an independent one-tailed or two-tailed independent Student's T-test with a 95% CI. A univariate regression analysis was used in Figure 2a.

Supplementary Material

Refer to Web version on PubMed Central for supplementary material.

Acknowledgements

We thank the Cedars-Sinai Genomics Core for RNA sequencing, the Cedars Sinai Biobank and Translational Research Core for tissue processing, Rebecca Benhaghnazar for technical assistance, and Alexandra Burtnick for help with Figure 7. Work in the Marbán lab was supported by NIH R01124074; work at Capricor Therapeutics was supported by DOD PRMRP PR150618.

References

1. Kreke M, Smith RR, Marban L and Marban E. Cardiospheres and cardiosphere-derived cells as therapeutic agents following myocardial infarction. Expert Rev Cardiovasc Ther. 2012;10:1185–94. [PubMed: 23098154]
2. Smith RR, Barile L, Cho HC, Leppo MK, Hare JM, Messina E, Giacomello A, Abraham MR and Marban E. Regenerative potential of cardiosphere-derived cells expanded from percutaneous endomyocardial biopsy specimens. Circulation. 2007;115:896–908. [PubMed: 17283259]
3. Aminzadeh MA, Rogers RG, Fournier M, Tobin RE, Guan X, Childers MK, Andres AM, Taylor DJ, Ibrahim A, Ding X, Torrente A, Goldhaber JM, Lewis M, Gottlieb RA, Victor RA and Marban E. Exosome-Mediated Benefits of Cell Therapy in Mouse and Human Models of Duchenne Muscular Dystrophy. Stem Cell Reports. 2018;10:942–955. [PubMed: 29478899]
4. Ashur C and Frishman WH. Cardiosphere-Derived Cells and Ischemic Heart Failure. Cardiol Rev. 2018;26:8–21. [PubMed: 29206745]
5. Oh H Cell Therapy Trials in Congenital Heart Disease. Circ Res. 2017;120:1353–1366. [PubMed: 28408455]
6. Chimenti I, Smith RR, Li TS, Gerstenblith G, Messina E, Giacomello A and Marban E. Relative roles of direct regeneration versus paracrine effects of human cardiosphere-derived cells transplanted into infarcted mice. Circ Res. 2010;106:971–80. [PubMed: 20110532]
7. Galvez BG, Covarello D, Tolorenzi R, Brunelli S, Dellavalle A, Crippa S, Mohammed SA, Scialla L, Cuccovillo I, Molla F, Staszewsky L, Maisano F, Sampaolesi M, Latini R and Cossu G. Human cardiac mesoangioblasts isolated from hypertrophic cardiomyopathies are greatly reduced in proliferation and differentiation potency. Cardiovasc Res. 2009;83:707–16. [PubMed: 19457891]
8. Salem B, Miner S, Hensel NF, Battiwalla M, Keyvanfar K, Stroncek DF, Gee AP, Hanley PJ, Bollard CM, Ito S and Barrett AJ. Quantitative activation suppression assay to evaluate human bone marrow-derived mesenchymal stromal cell potency. Cytotherapy. 2015;17:1675–86. [PubMed: 26422657]
9. Cheng K, Malliaras K, Smith RR, Shen D, Sun B, Blusztajn A, Xie Y, Ibrahim A, Aminzadeh MA, Liu W, Li TS, De Robertis MA, Marban L, Czer LSC, Trento A and Marban E. Human

cardiosphere-derived cells from advanced heart failure patients exhibit augmented functional potency in myocardial repair. JACC Heart Fail. 2014;2:49–61. [PubMed: 24511463]

10. Harvey E, Zhang H, Sepulveda P, Garcia SP, Sweeney D, Choudry FA, Castellano D, Thomas GN, Kattach H, Petersen R, Blake DJ, Taggart DP, Frontini M, Watt SM and Martin-Rendon E. Potency of Human Cardiosphere-Derived Cells from Patients with Ischemic Heart Disease Is Associated with Robust Vascular Supportive Ability. Stem Cells Transl Med. 2017;6:1399–1411. [PubMed: 28205406]
11. Marban E A mechanistic roadmap for the clinical application of cardiac cell therapies. Nature Biomedical Engineering. 2018;In press.
12. MacDonald BT, Tamai K and He X. Wnt/beta-catenin signaling: components, mechanisms, and diseases. Developmental cell. 2009;17:9–26. [PubMed: 19619488]
13. Cheng K, Ibrahim A, Hensley MT, Shen D, Sun B, Middleton R, Liu W, Smith RR and Marban E. Relative roles of CD90 and c-kit to the regenerative efficacy of cardiosphere-derived cells in humans and in a mouse model of myocardial infarction. J Am Heart Assoc. 2014;3:e001260. [PubMed: 25300435]
14. Vargas DA, Sun M, Sadykov K, Kukuruzinska MA and Zaman MH. The Integrated Role of Wnt/beta-Catenin, N-Glycosylation, and E-Cadherin-Mediated Adhesion in Network Dynamics. PLoS Comput Biol. 2016;12:e1005007. [PubMed: 27427963]
15. Lin X Functions of heparan sulfate proteoglycans in cell signaling during development. Development. 2004;131:6009–21. [PubMed: 15563523]
16. Barile L, Lionetti V, Cervio E, Matteucci M, Gherghiceanu M, Popescu LM, Torre T, Siclari F, Moccetti T and Vassalli G. Extracellular vesicles from human cardiac progenitor cells inhibit cardiomyocyte apoptosis and improve cardiac function after myocardial infarction. Cardiovasc Res. 2014;103:530–41. [PubMed: 25016614]
17. Ibrahim AG, Cheng K and Marban E. Exosomes as critical agents of cardiac regeneration triggered by cell therapy. Stem Cell Reports. 2014;2:606–19. [PubMed: 24936449]
18. May E, May P and Weil R. Analysis of the events leading to SV40-induced chromosome replication and mitosis in primary mouse kidney cell cultures. Proc Natl Acad Sci U S A. 1971;68:1208–11. [PubMed: 4331083]
19. Smith HS, Scher CD and Todaro GJ. Induction of cell division in medium lacking serum growth factor by SV40. Virology. 1971;44:359–70. [PubMed: 4105257]
20. Chen TS, Arslan F, Yin Y, Tan SS, Lai RC, Choo AB, Padmanabhan J, Lee CN, de Kleijn DP and Lim SK. Enabling a robust scalable manufacturing process for therapeutic exosomes through oncogenic immortalization of human ESC-derived MSCs. J Transl Med. 2011;9:47. [PubMed: 21513579]
21. Gillespie JR, Ulici V, Dupuis H, Higgs A, Dimattia A, Patel S, Woodgett JR and Beier F. Deletion of glycogen synthase kinase-3beta in cartilage results in up-regulation of glycogen synthase kinase-3alpha protein expression. Endocrinology. 2011;152:1755–66. [PubMed: 21325041]
22. Cambier L, Plate M, Sucov HM and Pashmforoush M. Nkx2–5 regulates cardiac growth through modulation of Wnt signaling by R-spondin3. Development. 2014;141:2959–71. [PubMed: 25053429]
23. Li H, Zuo S, He Z, Yang Y, Pasha Z, Wang Y and Xu M. Paracrine factors released by GATA-4 overexpressed mesenchymal stem cells increase angiogenesis and cell survival. Am J Physiol Heart Circ Physiol. 2010;299:H1772–81. [PubMed: 20870802]
24. Oh SY, Kim JY and Park C. The ETS Factor, ETV2: a Master Regulator for Vascular Endothelial Cell Development. Mol Cells. 2015;38:1029–36. [PubMed: 26694034]
25. Hofsteen P, Robitaille AM, Chapman DP, Moon RT and Murry CE. Quantitative proteomics identify DAB2 as a cardiac developmental regulator that inhibits WNT/beta-catenin signaling. Proc Natl Acad Sci U S A. 2016;113:1002–7. [PubMed: 26755607]
26. Palpant NJ, Pabon L, Roberts M, Hadland B, Jones D, Jones C, Moon RT, Ruzzo WL, Bernstein I, Zheng Y and Murry CE. Inhibition of beta-catenin signaling respecifies anterior-like endothelium into beating human cardiomyocytes. Development. 2015;142:3198–209. [PubMed: 26153229]

27. Wang Y, Lu P, Wu B, Riascos-Bernal DF, Sibinga NES, Valenta T, Basler K and Zhou B. Myocardial beta-Catenin-BMP2 signaling promotes mesenchymal cell proliferation during endocardial cushion formation. J Mol Cell Cardiol. 2018;123:150–158. [PubMed: 30201295]
28. Klaus A, Muller M, Schulz H, Saga Y, Martin JF and Birchmeier W. Wnt/beta-catenin and Bmp signals control distinct sets of transcription factors in cardiac progenitor cells. Proc Natl Acad Sci U S A. 2012;109:10921–6. [PubMed: 22711842]
29. Zelarayan L, Gehrke C and Bergmann MW. Role of beta-catenin in adult cardiac remodeling. Cell Cycle. 2007;6:2120–6. [PubMed: 17786052]
30. Ghosh-Choudhury N, Abboud SL, Chandrasekar B and Ghosh Choudhury G. BMP-2 regulates cardiomyocyte contractility in a phosphatidylinositol 3 kinase-dependent manner. FEBS Lett. 2003;544:181–4. [PubMed: 12782312]
31. Wang YX, Qian LX, Liu D, Yao LL, Jiang Q, Yu Z, Gui YH, Zhong TP and Song HY. Bone morphogenetic protein-2 acts upstream of myocyte-specific enhancer factor 2a to control embryonic cardiac contractility. Cardiovasc Res. 2007;74:290–303. [PubMed: 17367767]
32. Sun Q, Mao S, Li H, Zen K, Zhang CY and Li L. Role of miR-17 family in the negative feedback loop of bone morphogenetic protein signaling in neuron. PLoS One. 2013;8:e83067. [PubMed: 24349434]
33. Ning G, Liu X, Dai M, Meng A and Wang Q. MicroRNA-92a upholds Bmp signaling by targeting noggin3 during pharyngeal cartilage formation. Dev Cell. 2013;24:283–95. [PubMed: 23410941]
34. Nusse R Wnt signaling in disease and in development. Cell Res. 2005;15:28–32. [PubMed: 15686623]
35. Bukowska J, Ziecik AJ, Laguna J, Gawronska-Kozak B and Bodek G. The Importance of the Canonical Wnt Signaling Pathway in the Porcine Endometrial Stromal Stem/Progenitor Cells: Implications for Regeneration. Stem Cells Dev. 2015;24:2873–85. [PubMed: 26414529]
36. Cosin-Roger J, Ortiz-Masia D, Calatayud S, Hernandez C, Esplugues JV and Barrachina MD. The activation of Wnt signaling by a STAT6-dependent macrophage phenotype promotes mucosal repair in murine IBD. Mucosal Immunol. 2016;9:986–98. [PubMed: 26601901]
37. Li M, Chen H, Chen L, Chen Y, Liu X and Mo D. miR-709 modulates LPS-induced inflammatory response through targeting GSK-3beta. Int Immunopharmacol. 2016;36:333–8. [PubMed: 27232654]
38. Ortiz-Masia D, Cosin-Roger J, Calatayud S, Hernandez C, Alos R, Hinojosa J, Apostolova N, Alvarez A and Barrachina MD. Hypoxic macrophages impair autophagy in epithelial cells through Wnt1: relevance in IBD. Mucosal Immunol. 2014;7:929–38. [PubMed: 24301659]
39. Hsu YC, Chang PJ, Ho C, Huang YT, Shih YH, Wang CJ and Lin CL. Protective effects of miR-29a on diabetic glomerular dysfunction by modulation of DKK1/Wnt/beta-catenin signaling. Sci Rep. 2016;6:30575. [PubMed: 27460630]
40. Zhang GY, Wu LC, Liao T, Chen GC, Chen YH, Zhao YX, Chen SY, Wang AY, Lin K, Lin DM, Yang JQ, Gao WY and Li QF. A novel regulatory function for miR-29a in keloid fibrogenesis. Clin Exp Dermatol. 2016;41:341–5. [PubMed: 26566758]
41. Chilosi M, Calio A, Rossi A, Gilioli E, Pedica F, Montagna L, Pedron S, Confalonieri M, Doglioni C, Ziesche R, Grubinger M, Mikulits W and Poletti V. Epithelial to mesenchymal transition-related proteins ZEB1, beta-catenin, and beta-tubulin-III in idiopathic pulmonary fibrosis. Mod Pathol. 2016.
42. Wang S, Ye L, Li M, Liu J, Jiang C, Hong H, Zhu H and Sun Y. GSK-3beta Inhibitor CHIR-99021 Promotes Proliferation via Upregulating beta-catenin in Neonatal Atrial Human Cardiomyocytes. J Cardiovasc Pharmacol. 2016.
43. Ni W, Lin C, Guo L, Wu J, Chen Y, Chai R, Li W and Li H. Extensive Supporting Cell Proliferation and Mitotic Hair Cell Generation by In Vivo Genetic Reprogramming in the Neonatal Mouse Cochlea. J Neurosci. 2016;36:8734–45. [PubMed: 27535918]
44. D'Uva G, Aharonov A, Lauriola M, Kain D, Yahalom-Ronen Y, Carvalho S, Weisinger K, Bassat E, Rajchman D, Yifa O, Lysenko M, Konfino T, Hegesh J, Brenner O, Neeman M, Yarden Y, Leor J, Sarig R, Harvey RP and Tzahor E. ERBB2 triggers mammalian heart regeneration by promoting cardiomyocyte dedifferentiation and proliferation. Nat Cell Biol. 2015;17:627–38. [PubMed: 25848746]

45. Potz BA, Sabe AA, Elmadhun NY, Clements RT, Robich MP, Sodha NR and Sellke FW. Glycogen Synthase Kinase 3beta Inhibition Improves Myocardial Angiogenesis and Perfusion in a Swine Model of Metabolic Syndrome. J Am Heart Assoc. 2016;5.
46. Birdsey GM, Shah AV, Dufton N, Reynolds LE, Osuna Almagro L, Yang Y, Aspalter IM, Khan ST, Mason JC, Dejana E, Gottgens B, Hodivala-Dilke K, Gerhardt H, Adams RH and Randi AM. The endothelial transcription factor ERG promotes vascular stability and growth through Wnt/beta-catenin signaling. Dev Cell. 2015;32:82–96. [PubMed: 25584796]
47. Kim KI, Cho HJ, Hahn JY, Kim TY, Park KW, Koo BK, Shin CS, Kim CH, Oh BH, Lee MM, Park YB and Kim HS. Beta-catenin overexpression augments angiogenesis and skeletal muscle regeneration through dual mechanism of vascular endothelial growth factor-mediated endothelial cell proliferation and progenitor cell mobilization. Arterioscler Thromb Vasc Biol. 2006;26:91–8. [PubMed: 16254206]
48. Li J, Xuan W, Yan R, Tropak MB, Jean-St-Michel E, Liang W, Gladstone R, Backx PH, Kharbanda RK and Redington AN. Remote preconditioning provides potent cardioprotection via PI3K/Akt activation and is associated with nuclear accumulation of beta-catenin. Clin Sci (Lond). 2011;120:451–62. [PubMed: 21143191]
49. Hahn JY, Cho HJ, Bae JW, Yuk HS, Kim KI, Park KW, Koo BK, Chae IH, Shin CS, Oh BH, Choi YS, Park YB and Kim HS. Beta-catenin overexpression reduces myocardial infarct size through differential effects on cardiomyocytes and cardiac fibroblasts. J Biol Chem. 2006;281:30979–89. [PubMed: 16920707]
50. Marban E The Secret Life of Exosomes: What Bees Can Teach Us About Next-Generation Therapeutics. J Am Coll Cardiol. 2018;71:193–200. [PubMed: 29325643]
51. Dodson BP and Levine AD. Challenges in the translation and commercialization of cell therapies. BMC Biotechnol. 2015;15:70. [PubMed: 26250902]
52. Akers JC, Ramakrishnan V, Yang I, Hua W, Mao Y, Carter BS and Chen CC. Optimizing preservation of extracellular vesicular miRNAs derived from clinical cerebrospinal fluid. Cancer Biomark. 2016;17:125–32. [PubMed: 27062568]
53. Ibrahim A and Marban E. Exosomes: Fundamental Biology and Roles in Cardiovascular Physiology. Annu Rev Physiol. 2016;78:67–83. [PubMed: 26667071]
54. Liu B, Lee BW, Nakanishi K, Villasante A, Williamson R, Metz J, Kim J, Kanai M, Bi L, Brown K, Di Paolo G, Homma S, Sims PA, Topkara VK and Vunjak-Novakovic G. Cardiac recovery via extended cell-free delivery of extracellular vesicles secreted by cardiomyocytes derived from induced pluripotent stem cells. Nat Biomed Eng. 2018;2:293–303. [PubMed: 30271672]
55. Cambier L, de Couto G, Ibrahim A, Echavez AK, Valle J, Liu W, Kreke M, Smith RR, Marban L and Marban E. Y RNA fragment in extracellular vesicles confers cardioprotection via modulation of IL-10 expression and secretion. EMBO Mol Med. 2017;9:337–352. [PubMed: 28167565]
56. Gallet R, Dawkins J, Valle J, Simsolo E, de Couto G, Middleton R, Tseliou E, Luthringer D, Kreke M, Smith RR, Marban L, Ghaleh B and Marban E. Exosomes secreted by cardiosphere-derived cells reduce scarring, attenuate adverse remodelling, and improve function in acute and chronic porcine myocardial infarction. Eur Heart J. 2017;38:201–211. [PubMed: 28158410]

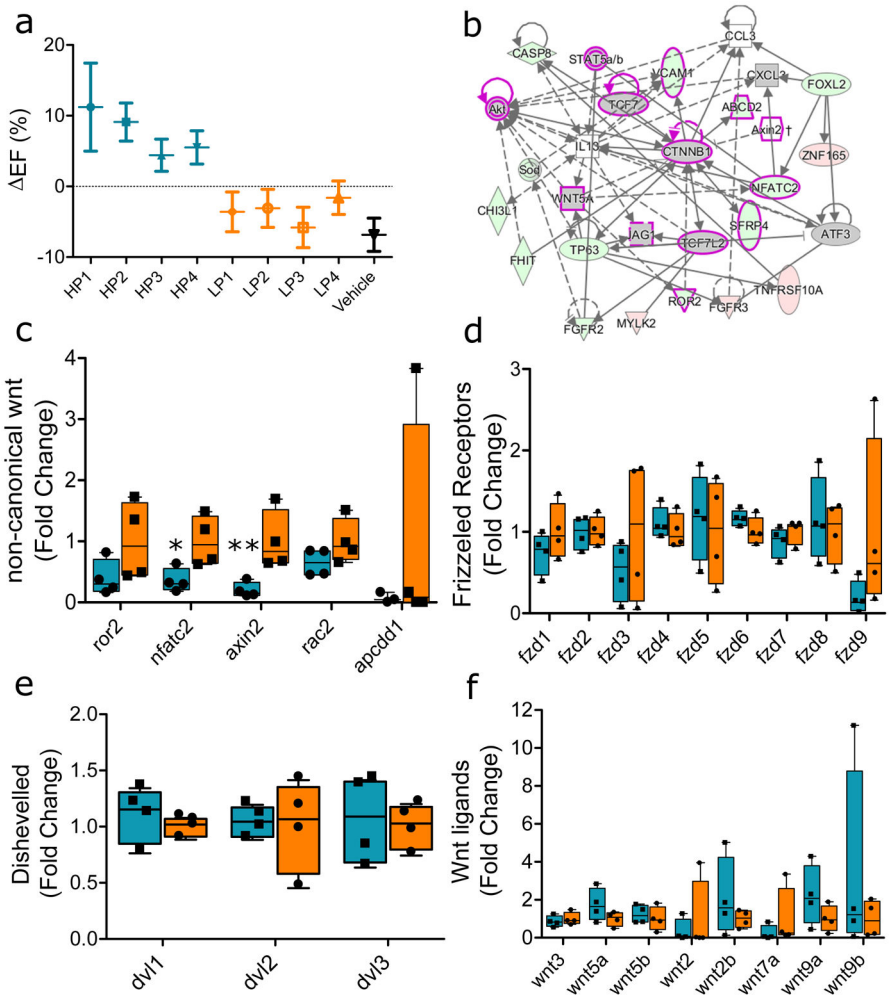

Fig. 1 |. Sequencing summary of high- and low-potency donors

(a) Potency was determined based on the ability of CDCs to improve global heart function in a mouse model of myocardial infarction (n=7 animals/group; error bars represent SD). (b) Ingenuity pathway analysis showing predicted activation of the canonical Wnt/β-catenin pathway. Shapes indicate the type of molecule (e.g. transcription factor, cytoplasmic protein, cytokine). Red indicates upregulation by sequencing while green signifies downregulation. Gray means no significant fold change by sequencing, but the β-catenin pathway was identified by IPA to be activated (post transcriptionally) given the differential expression of its signaling partners. The magenta frame signifies signaling partners in the Wnt/β-catenin pathway. Arrows indicate activation, stop lines signify inhibition. (c) Decreased expression of non-canonical Wnt signaling markers in HP vs. LP CDC donors (*p=0.014, **p=0.009,). Equivalent expression of (d) Frizzled receptors, (e) Dishevelled, and (f) Wnt ligand genes between both groups of CDCs. (1c-1f n=4 different donors/group; error bars represent min and max) 95% CI using one-sided Student's independent t-test. For box plots, bar-ends define the range of the data, box-ends the interquartile range, and central bars are median values.

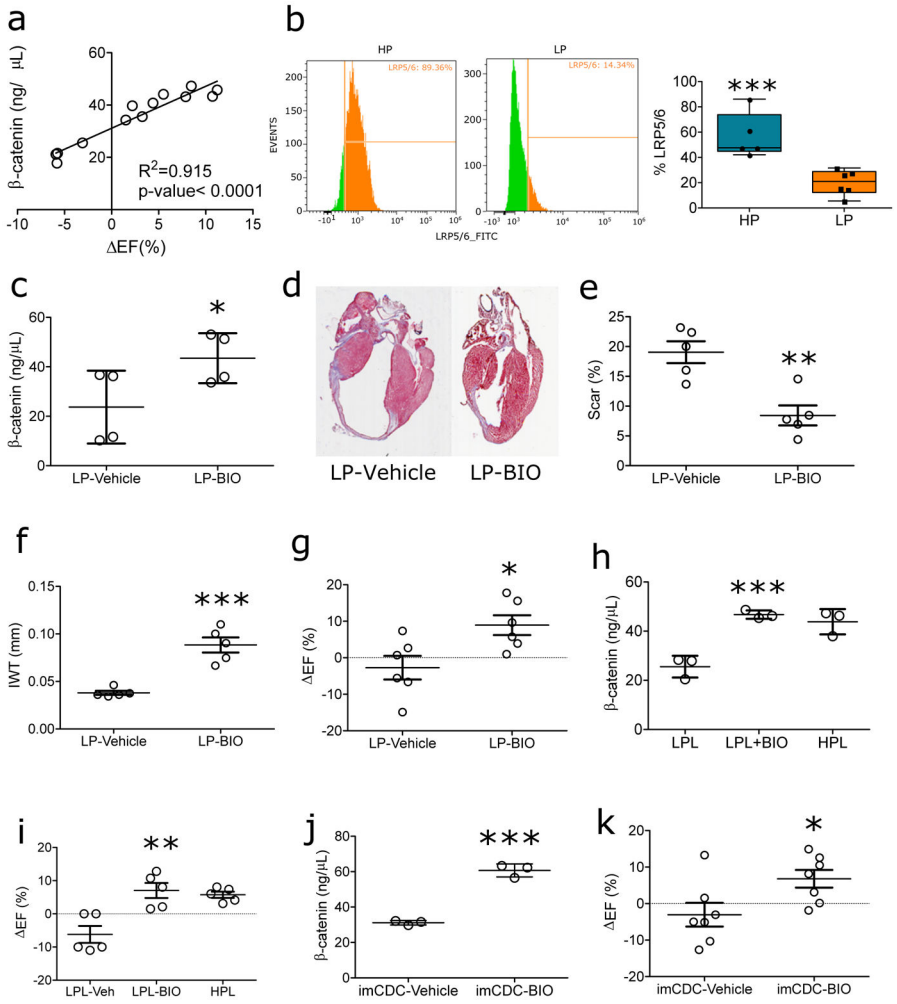

Fig. 2 |. β-catenin is necessary for CDC potency.

(**a**) Correlation between total β-catenin levels in donor CDCs (*n*=13) and therapeutic performance (expressed as change in left ventricular ejection fraction) *in vivo*. (**b**) Higher expression of the Wnt coreceptor LRP5/6 in high-potency CDCs (HP) compared with low-potency CDCs (LP; *n*=5 different donors per group; error bars represent min and max, ***p <0.001). (**c**) Exposing LP CDCs to 5 μM BIO increased β-catenin levels (n= 2 independent experiments and represented as mean ±SD, *p=0.032) and restored therapeutic efficacy (**d-g**): Percent scar was determined using image J quantification from Masson trichrome stained sections (n=5 animals per group; data presented as mean ± SEM) including percent scar (**p=0.001), and infarct wall thickness (***p>0.001). Functional improvement as seen by increased ejection fraction was also observed (*n*=6 animals per group; data represented as mean ± SEM, *p=0.01). These results were further confirmed in CDCs from a low potency lot from a sometimes-potent CDC source (LPL), as BIO exposure restored potency to levels similar to potent lots from the same donor (**h**; n= 3 replicates per group, data represented as mean ± SD ***p<0.001, **i**; *n*=5 animals per group; data represented as mean ± SEM **p=0.002). Restoration of β-catenin levels (**j**; n= 3 replicates per group, data represented as mean ± SD ***p<0.001) also rescued potency in CDCs that were immortalized (SV40-T+t)

with diminished potency (imCDC) (**k**; n=7 animals per group; data represented as mean ± SEM, *p=0.016). Statistical analysis: 95% CI using one-sided Student's Independent t-test. For box plots, bar-ends define the range of the data, box-ends the interquartile range, and central bars are median values.

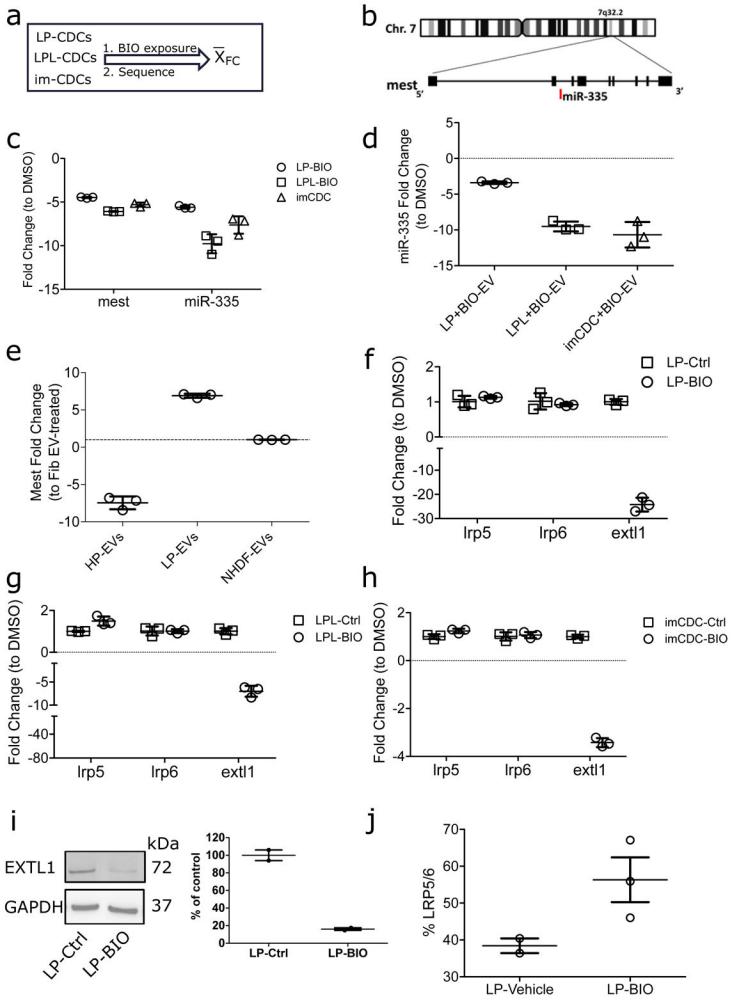

Fig. 3 |. Mest regulates β-catenin in CDCs.

(**a**) Experimental schematic. RNA from three pairs of cells was sequenced: CDCs from a low-potency donor (LP), CDCs from a low-potency lot from an otherwise potent donor (LPL), and CDCs with diminished potency due to immortalization (imCDC). Differential expression analysis was made within each group (BIO exposed versus vehicle control) and results (expressed in fold change) were averaged among the three groups. (**b**) Sequencing identified the β-catenin regulator mesoderm specific transcript (mest) and its cognate micro RNA (miR-335) are downregulated. (**c**) qPCR validation of the changes in mest and miR-335 (n= 3 replicates; data presented as mean ± SD). (**d**) Fold change in gene expression of miR-335 in extracellular vesicles (EVs) isolated from LP, LPL, and imCDC exposed to BIO compared with their vehicle control counterparts (n= 3 replicates; data presented as mean ±SD). (**e**) EVs from highly potent CDC EVs decrease mest in fibroblasts (n= 3 replicates; data presented as mean ±SD). (**f-h**) QPCR verification of the Wnt signaling co-receptor, LRP5/6, and a member of the exostosin family glucosyltransferases EXTL1 in BIO-exposed LP. LPL, and imCDCs (n= 3 replicates; data presented as mean ±SD ***p<0.001 for all pairs). (**i**) Verification of EXTL1 protein downregulation in LP cells following BIO exposure (n= 3 replicates; data presented as mean ±SD). (**j**) Flow cytometry

of BIO exposure to LP increased LRP5/6 level n=3 independent experiments; data presented as mean ±SD). Statistical analysis: 95% CI using one-sided Student's independent t-test.

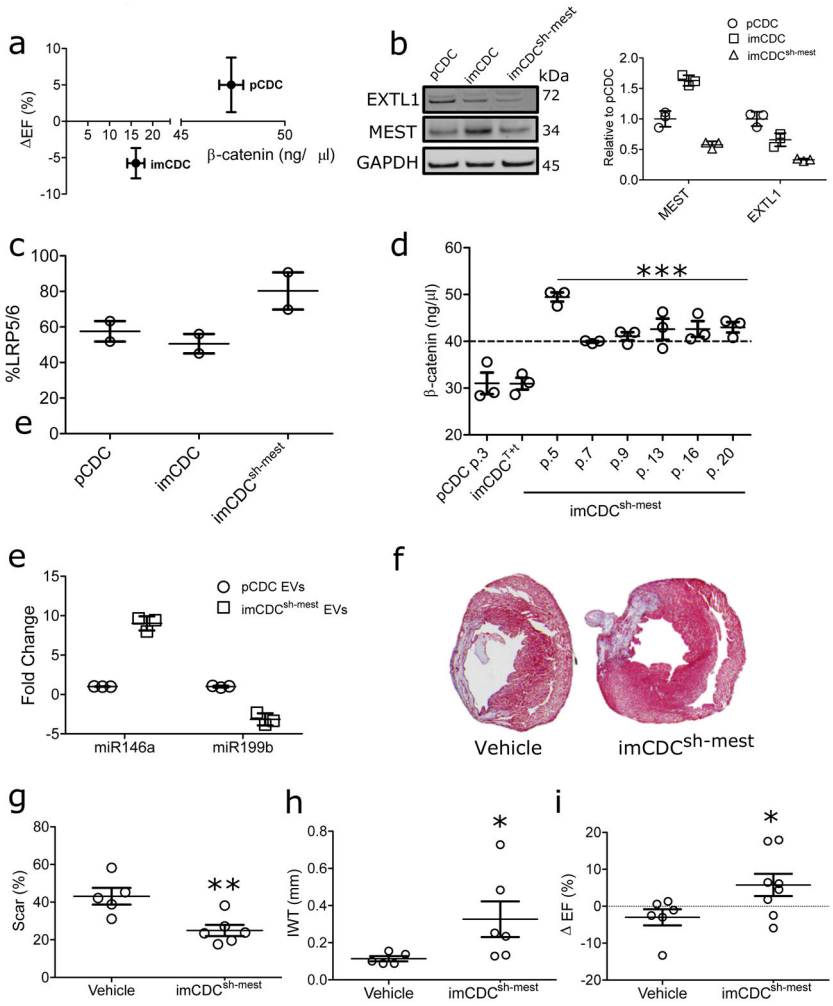

Fig. 4 |. Mest inhibition in immortalized CDCs.

(**a**) Lentiviral transduction of SV40 T+t transgene leads to immortalization but attenuation of β-catenin levels and therapeutic efficacy *in vivo* as β-catenin ELISA and change in left ventricular functional improvement (ΔEF) in a mouse MI model. (n=7 animals/group: data presented as mean ±SD) (**b**) Western blot and pooled data of EXTL1 and mest protein levels in primary CDCs (pCDC) and modified immortalized CDCs (imCDC$^{sh\text{-}mest}$; n=3 biological replicates/group; data presented as mean ±SD). (**c**) Flow cytometry of LRP5/6 increased in imCDC$^{sh\text{-}mest}$ compared with pCDC (n=2 independent experiments; data presented as mean ± SD). (**d**) Successful maintenance of β-catenin protein levels over several passages after immortalization is coupled with a small hairpin-mediated knockdown of mest (data represents 3 independent experiments n= 3 replicates per group; mean ±SD, p<0.001 using One Way ANOVA with Dunnets post-test). The dotted line at 40 ng/μl represents the mean β-catenin level among highly potent donors. (**e**) qPCR of miR146a and miR199b in EVs of pCDC and imCDC$^{sh\text{-}mest}$ (n=.3 replicates per group; data presented as mean ±SD) Performance of imCDC$^{sh\text{-}mest}$ and pCDC in mouse models of acute MI (n=7 animals/group; data presented as mean ±SEM, p), including structural improvement in scar size (**g**; data presented as ±SEM **p=0.003) and infarct wall thickness (**h**; data presented as ±SEM,

*p=0.038) and functional improvement (**i**; data presented as ±SEM *p=0.024). Statistical analysis: 95% CI using one-sided Student's Independent t-test.

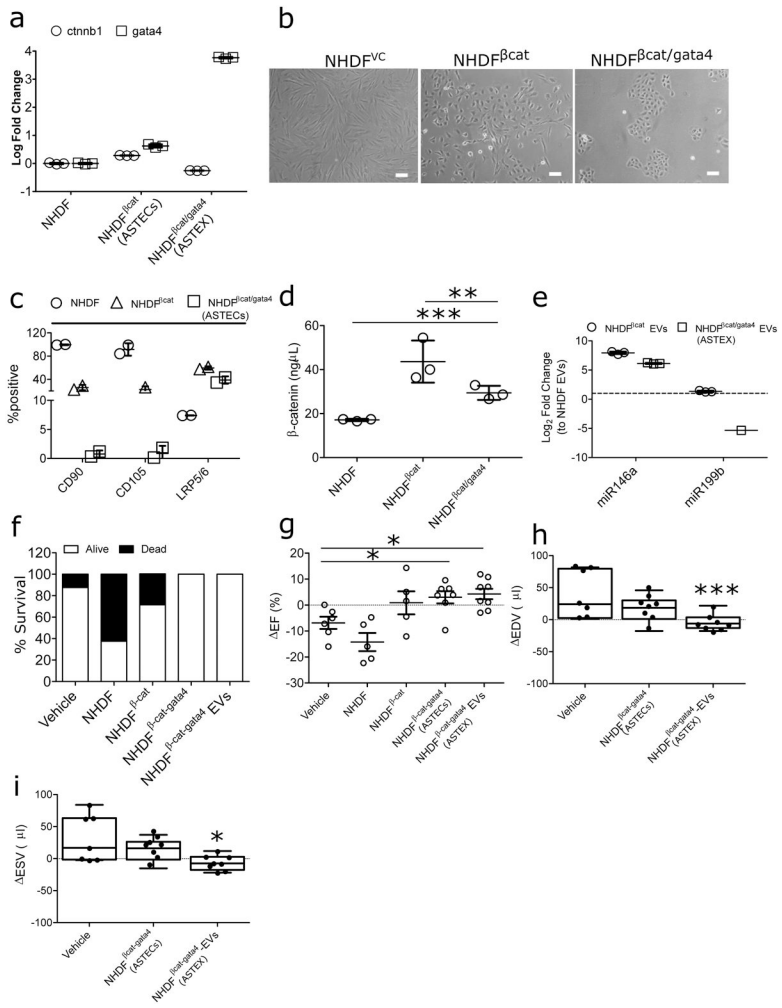

Fig. 5 |. NHDF immortalization with β-catenin or β-catenin/gata4.

(**a**) qPCR verification of β-catenin or β-catenin/gata4 in the transduced cells. (**b**) Cell morphology changed after transduction. NHDF$^{\beta cat}$ and NHDF$^{\beta cat/gata4}$ became more endothelial-like and epithelial-like, respectively. (**c**) Flow cytometry of CD90, CD105, and LRP5/6 in NHDF, NHDF$^{\beta cat}$ and NHDF$^{\beta cat/gata4}$ (n=2 biological replicates per group; data presented as mean ± SD). (**d**) ELISA of β-catenin level after transduction (n=3 biological replicates per group). (**e**) qPCR of microRNA markers in the extracellular vesicles of transduced cells (n=3 replicates per group; only 1 of the 3 replicates in miR199b was detectable). (**f-i**) Mortality is enhanced in myocardial infarction mice injected with NHDFs. However, animals given NHDFs transduced with β-catenin or β-catenin and gata4 leads to improved mortality (**f**), functional improvement (**g**; n= 7 animals/group, data presented as mean ± SEM, *p=0.033) and attenuation of remodeling like those observed in CDCs and CDC EVs. (EDV, **h**; error bars represent min and max, ***p=0.0094; ESV, **i**; error bars represent min and max, *p=0.019) Scale bar: 100 μm. Statistical analysis: *p<0.05, **p<0.01, Statistical Analysis: 95% CI using one-sided Student's Independent t-test or one-way ANOVA with Dunnet's post-test for multiple comparisons. For box plots, bar-ends

define the range of the data, box-ends the interquartile range, and central bars are median values.

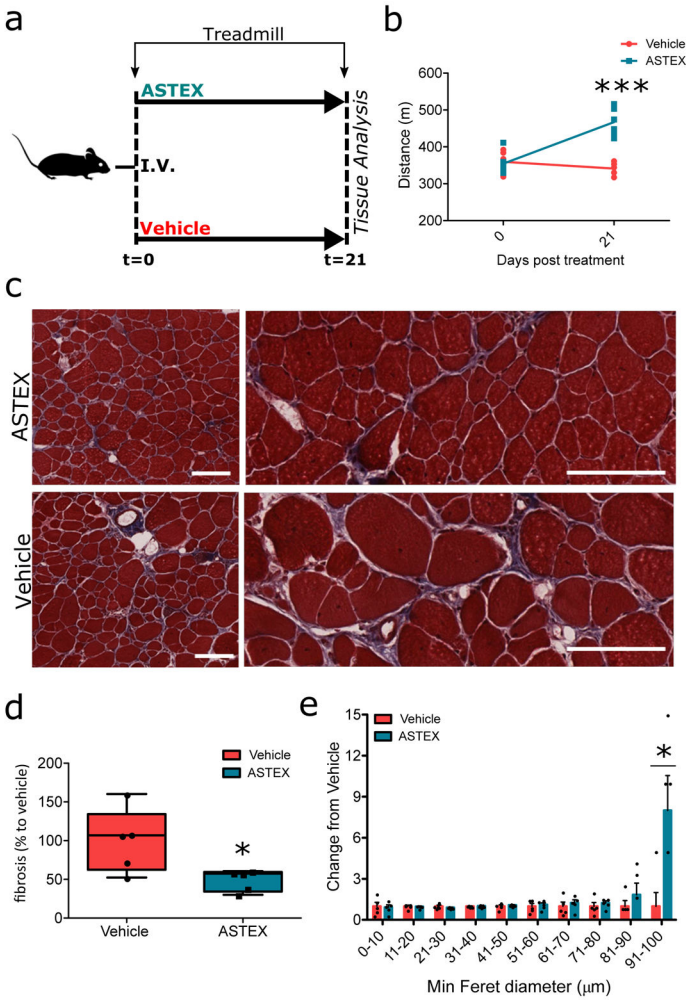

Fig. 6 |. Bioactivity of ASTEX in an *mdx* mouse model of Duchenne muscular dystrophy.

(**a**) Schematic of the experimental design. Mice underwent graded exercise testing, then were injected with ASTEX or vehicle control (IMDM) into the femoral vein. Exercise testing was repeated 3 weeks later. (**b**) Maximal exercise capacity was significantly improved in ASTEX-injected *mdx* mice after 3 weeks (n=5 per group; data presented as mean ±SEM. ***p<0.001). (**c**) Representative Masson's trichrome stained micrographs from vehicle and ASTEX-injected *mdx* TA muscles. Pooled data from **c** indicate less muscle fibrosis in *mdx* TA muscles three weeks after ASTEX injection (n=5 animals per group; data presented as mean with min and max, *p=0.015). (**d**) Pooled data from 1,000 analyzed myofibers per muscle in (**e**) indicate ASTEX shifted the myofiber size distribution to larger diameters (n=5 per group; data presented as mean ±SEM, *p=0.017). (**c**) Scale bars: 100 μm. Statistical analysis: 95% CI using Student's Independent t-test. For box plots, bar-ends define the range of the data, box-ends the interquartile range, and central bars are median values.

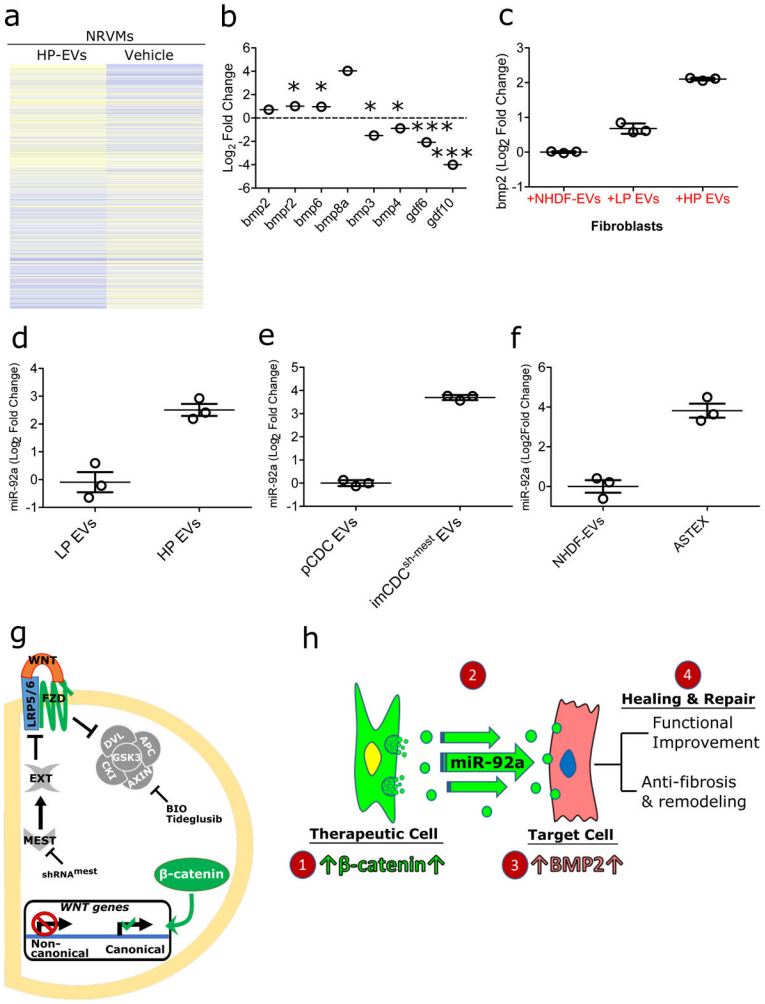

Fig. 7 |. β-catenin-activation leads to downstream activation of bmp2 in target cells via miR-92a.

(a) Heat map of differentially expressed genes in neonatal rat ventricular myocytes exposed to HP EVs compared to control (b) Upregulation of anti-fibrotic and downregulation of pro-fibrotic members of the bmp family members in HP EV-exposed myocytes (statistical analysis done using likelihood ratio test using a Chi-squared distribution). (c) Enrichment of miR-92a in HP-EVs compared to LP EVs (n=3 different donor EVs per group; data presented as mean ± SEM ***p<0.001). (d) Exposure of fibroblasts to EVs from HP cells leads to increased bmp2 expression (n=3 replicates per group; data presented as mean ± SD). (e, f) Consistent with potency, EVs isolated from imCDC^{shmest} and ASTEX are enriched in miR-92a compared to primary CDC EVs and fibroblast EVs respectively (n=3 replicates/ group; data presented as mean ± SD) (g) Mest is the turning point between non-canonical wnt and canonical wnt signal pathway, which is a critical determinant for therapeutic cell potency. (h) Schematic of working hypothesis. β-catenin activation in CDCs leads to enrichment of miR-92a in secreted EVs. Secreted EVs are uptaken by target cells, activate bmp2 signalling leading to healing and repair.